agriculture

MDPI

Article

Spatiotemporal Integration of Time-Series Remote Sensing and Soil Attributes for Precision Management Zoning in Daylily Cultivation

Liang Han [1,2,3,*], Jianwen Duan [2,3], Gaoyi Ji [1,2], Xudong Li [1,2], Nan Zhang [1,2] and Baoxing Liang [4]

[1] College of Architecture and Geomatics Engineering, Shanxi Datong University, Datong 037003, China
[2] Key Laboratory of Unmanned Aerial Vehicle Remote Sensing Technology and Applications of Datong City, Datong 037003, China
[3] Shanxi Province Doctoral Innovation Workstation, Shanxi Wanding Space Digital Co., Ltd., Datong 037008, China
[4] Shanxi Technical Innovation Center for Comprehensive Monitoring and Emergency Disaster Reduction in Mining Areas, Shanxi Provincial Coal Geology 115 Exploration Institute Co., Ltd., Datong 037003, China
* Correspondence: hanjabolgo@sxdtdx.edu.cn

Abstract

Effective management zone delineation is key to implementing site-specific strategies that address spatiotemporal heterogeneity in agriculture. Although time-series remote sensing offers a dynamic perspective, most current methods lack the framework to integrate it with soil properties, thereby hindering accurate characterization of crop growth variability. This study bridges the gap by developing a spatiotemporal framework that synthesizes remote sensing-derived phenology and soil attributes for daylily management zoning. Through a sequential approach—phenological metric extraction, SNIC-based segmentation, and STSF classification—we produce refined phenological time-series stacks. These outputs are designed to elucidate the drivers of field heterogeneity and directly inform precision management strategies. Compared to pixel-based and SNIC-based random forest, the STSF–SNIC framework increased spatial overlap rates by 5.4–8.0% (reaching 88.6%), despite comparable overall accuracy and kappa coefficients (OA/kappa: 92–94%). Geographical detector analysis identified village boundaries, soil type, total nitrogen, and organic carbon as key drivers of spatial patterns. A spatial generalized fuzzy c-means model, incorporating crop growth dynamics and soil gradients, reduced management zone fragmentation by 27.8% compared to conventional methods, with spatial autocorrelation analysis confirming enhanced spatial consistency (Moran's I = 0.600 vs. 0.433, $p < 0.001$). In conclusion, by integrating time-series remote sensing phenology with soil attribute analysis within a spatially constrained clustering scheme, this study (1) provides a novel method for delineating coherent management zones, (2) reveals key drivers of crop growth heterogeneity, and (3) demonstrates a transferable pathway for translating satellite data into precision management actions. It thereby exemplifies the value of applied remote sensing in addressing practical challenges in sustainable agriculture.

Keywords: daylily; management zone; growth heterogeneity; soil gradients; time-series classification

Check for updates

Academic Editor: Ezio Riggi

Received: 18 December 2025
Revised: 9 January 2026
Accepted: 10 January 2026
Published: 27 February 2026

Copyright: © 2026 by the authors. Licensee MDPI, Basel, Switzerland. This article is an open access article distributed under the terms and conditions of the Creative Commons Attribution (CC BY) license.

1. Introduction

The sustainable intensification of agricultural systems is critical for addressing global food security challenges under changing environmental conditions. In this context, spe-

cialty crops with high nutritional and economic value, such as daylily (Hemerocallis citrina Baroni), play a significant role in supporting rural livelihoods and healthy food systems. According to the "2023 White Paper on Daylily Industry Development", China has cultivated daylilies across approximately 69,300 hectares, demonstrating its wide adaptability to diverse climatic conditions [1]. As a nutrient-dense crop rich in proteins, vitamins, and essential amino acids, daylily holds substantial market potential and contributes to nutritional security [2]. However, realizing its full socioeconomic benefits requires overcoming persistent monitoring and management challenges. Remote sensing offers a promising alternative to current monitoring practices, which rely predominantly on subjective farmer experience or spatially limited fixed-point observations. These conventional approaches are prone to bias and fail to capture field-scale spatial heterogeneity [3]. Furthermore, the absence of long-term, dynamic data hinders the analysis of crop-environment interactions and the design of sustainable cultivation strategies [4]. However, the application of remote sensing to daylilies is challenged by its distinctive phenology. Unlike cereal crops with a single, well-defined harvest, daylilies undergo repeated and overlapping bud-production cycles during an extended harvest window. Consequently, its canopy structure is dynamic and heterogeneous. A key characteristic is the co-occurrence of active vegetative growth and continuous reproductive development. This complex phenological expression complicates accurate monitoring using conventional remote sensing methodologies.

The imperative for precision management in daylily cultivation is acute. Yield and quality are highly sensitive to spatial variability in soil moisture, nutrient availability, and microclimate, especially across topographically complex terrains. Uniform management leads to significant inefficiencies and environmental losses. Therefore, accurately zoning management units based on both intrinsic (soil properties) and dynamic (growth heterogeneity) drivers is paramount. The management zone (MZ) is a subfield region delineated by spatial heterogeneity in soil attributes, crop growth patterns, and historical yield data [5,6]. MZ design helps optimize resource use, reduce environmental impacts, and enhance agricultural productivity, forming a core component of precision agriculture. Previous studies show a robust correlation between productivity and the satellite-derived Normalized Difference Vegetation Index (NDVI). Thus, NDVI data are efficient substitutes for or complements to productivity maps for delimiting MZ, especially when direct measurements are unavailable, thereby enhancing practicality in resource-limited contexts [7–9]. Common methods for MZ delineation include fuzzy c-means clustering, k-means, and quintile classification [7,9,10]. However, these conventional techniques frequently ignore spatial autocorrelation, a fundamental characteristic of agricultural variables. As a result, they may produce spatially fragmented zones that are impractical for field management and increase operational complexity [11]. In parallel, accurate crop identification is a prerequisite for reliable growth monitoring and MZ delineation. The synergistic integration of multisource remote-sensing data, time-series analysis, and object-oriented segmentation techniques has substantially advanced crop identification [12–17].

To address these challenges, this study introduces an integrated analytical framework. This framework is designed to (i) decipher complex temporal signatures using a Supervised Time-Series Forest (STSF) classifier, which identifies subtle phenological patterns in daylily from multispectral index data; (ii) enhance spatial consistency and suppress noise by applying Simple Non-Iterative Clustering (SNIC) to multi-temporal, multi-source imagery prior to classification; and (iii) bridge precise field mapping with actionable management zoning by integrating Geographical Detector analysis and spatially constrained clustering to delineate zones based on key driving factors.

2. Materials and Methods

2.1. Study Areas

Yunzhou district is situated in Datong City in north China's Shanxi province (39°43′ N–40°16′ N, 113°20′ E–113°55′ E) on the eastern edge of the Loess Plateau. It covers an area of 1478 km^2, including nine towns (Figure 1). The terrain is high in the north and south, low in the middle, and inclined from northwest to southeast, with an elevation ranging from 900 to 2100 m. The Sanggan River flows across the plain and converges into the Cetian Reservoir. The Yunzhou district is in a warm temperate zone with a semiarid continental monsoon climate. The mean annual temperature and precipitation are 6.4 °C and 391.5 mm. The zone includes various landscapes, such as water bodies, grasslands, wetlands, forests, cropland, and photovoltaic power stations. The agricultural landscape is managed extensively to produce various crops with heterogeneous management practices and agricultural schedules. The principal food crops in Yunzhou District are maize, potatoes, and daylilies.

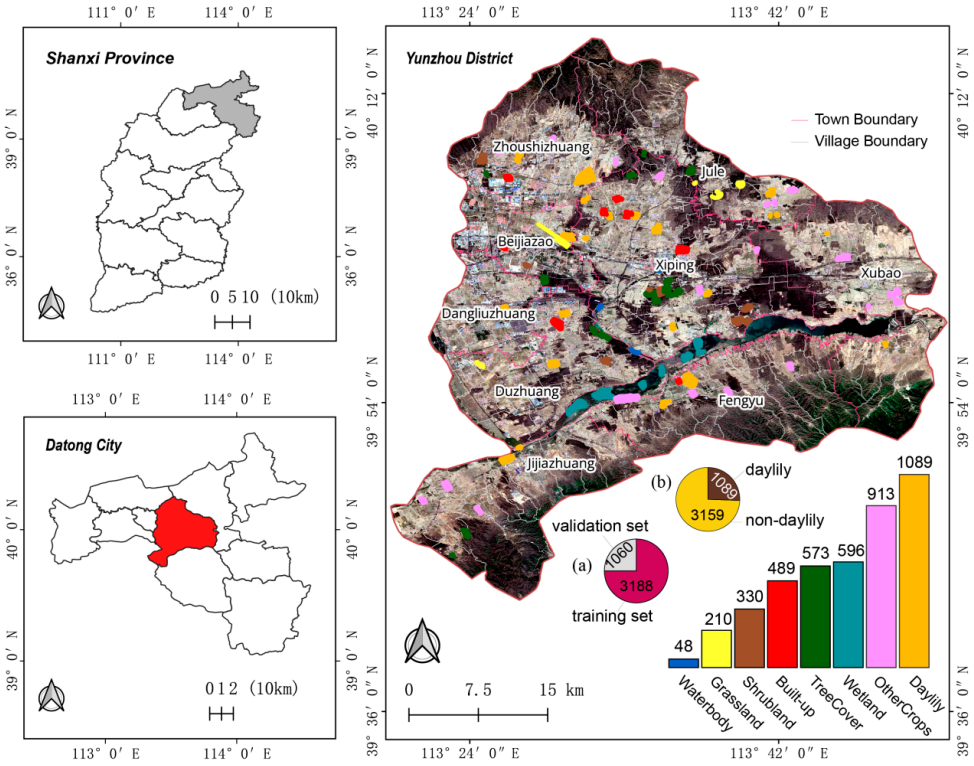


Figure 1. Study area map with spatial distribution of training and validation samples. The right panel displays Yunzhou district's remote sensing imagery in true-color composite during the spring-seedling growth stage of daylily cultivation. Two pie charts depict the following: (**a**) the ratio of training to validation samples (70%:30%), and (**b**) the classification balance between positive (daylily-classified) and negative samples. The adjacent bar chart summarizes sample point counts across eight land cover categories.

Daylilies are low-maintenance, drought-resistant herbaceous perennial plants that grow in diverse soils and are not susceptible to pests and diseases. They grow in five distinct stages: the spring-seedling stage, bolting-budding stage, flowering stage (picking stage), autumn-seedling stage, and winter-dormant stage. Daylily buds are picked from late June until early August (before flowering), usually between 5 and 10 am.

2.2. Data Acquisition and Processing

2.2.1. Sentinel-1 Imagery

Sentinel-1 provides C-band synthetic aperture radar (SAR) imagery in dual-polarization (VV and VH) at a spatial resolution of 10 m, with a nominal revisit frequency of 12 days. In this study, we used Level-1 Ground Range Detected (GRD) products acquired in Interferometric Wide (IW) swath mode from ascending orbits. All available scenes covering the primary growing stages of daylily in the study area were collected (Table 1). Preprocessing was conducted within the Google Earth Engine (GEE) platform using a custom script. The procedure included converting backscatter intensity to decibels (dB), applying a speckle filter to reduce radar noise, and performing terrain correction to account for topographic effects. Previous studies have shown that cross-polarized VH backscatter is generally more sensitive to vegetation structure, density, and phenological status than co-polarized VV [18]. Accordingly, VH backscatter has proven more effective for distinguishing among land cover types such as forest, grassland, and cropland [19]. For these reasons, the VH polarization was primarily used in the subsequent analysis.

Table 1. Temporal distribution and quantity of remote sensing imagery across growth stages.

	T1 (20 March–30 April)	**T2 (20 May–25 June)**	**T3 (1 July–15 August)**	**T4 (21 August–25 September)**	**T5 (1 October–31 October)**
S1	7	6	6	6	5
S2	55	65	86	62	44

Note: S1, Sentinel-1 SAR; S2, Sentinel-2 MSI; T1, spring-seedling stage; T2, bolting-budding stage; T3, picking stage; T4, post-picking stage; T5, autumn-seedling stage.

2.2.2. Sentinel-2 Imagery

Sentinel-2 provides free public multispectral data with a spatial resolution from 10 to 60 m and 13 spectral bands from 440 to 2200 nm. With the constellation of Sentinel-2A and -2B, the combined revisit frequency is approximately 5 days under optimal orbital configuration. All available scenes over the study area during the daylily growing season were acquired and processed after cloud masking. Within GEE, a time series of three key vegetation indices (Table S1) was computed: the Normalized Difference Vegetation Index (NDVI), the Plant Senescence Reflectance Index (PSRI), and the Chlorophyll Vegetation Index (CVI). This specific combination was chosen to form a complementary suite capturing distinct physiological dimensions: NDVI for general canopy greenness and biomass dynamics, CVI for chlorophyll content and photosynthetic vigor (closely linked to bud development), and PSRI for subtle senescence-related pigment changes indicative of bud maturation. This synergistic approach enables a holistic phenological assessment while minimizing redundancy among indices.

2.2.3. Elevation, Precipitation, Temperature, and Soil Raster Data

The shuttle radar topography mission (SRTM) digital elevation model (DEM) provided by NASA has a resolution of 1 arc-second (approximately 30 m). The GEE downloaded and clipped the SRTM digital elevation model within the Yunzhou District. The 1 km monthly mean temperature and precipitation raster data for China from March to October 2022 were acquired from the National Tibetan Plateau Data Center [20,21].

The Harmonized World Soil Database version 2.0 (HWSD v2.0) provided the soil raster image, which offers 1 km resolution information on soil properties, including their morphological, chemical, and physical characteristics. According to the classification provided by the Food and Agriculture Organization of the United Nations (FAO), the Yunzhou district's soil type is 47.4% calcaric cambisols. Other notable soil categories include haplic Kastanozem (25.6%), eutric regosol (8.5%), salic fluvisol (7.0%), and calcaric

fluvisol (4.8%). Total nitrogen content serves as a fundamental metric for evaluating soil fertility and plant nutrient availability. High nitrogen levels generally indicate a more fertile soil capable of supporting vigorous plant growth. In HWSD v2.0, the total nitrogen content is commonly reported in grams per kilogram (g/kg), reflecting the proportion of nitrogen relative to the total soil mass. Organic carbon content gives the amount of organic matter in the soil, which is crucial for soil structure, fertility, and biological activity. Finally, organic matter improves soil texture, water retention, and nutrient availability, which enhances soil health and productivity. To align these 1 km resolution raster datasets with the 10 m resolution Sentinel-1/Sentinel-2 imagery, this study resampled them to a 10 m grid using bilinear interpolation.

2.2.4. Composite Data and Processing

We chose temporal images with cloud coverage of less than 50% spanning from 2022 to 2023. The selection criteria were based on the phenology of daylilies, with images taken from 20 March to 30 April designated as T1, 20 May to 25 June as T2, 1 July to 15 August as T3, 21 August to 25 September as T4, and 1 October to 31 October as T5. Table 1 gives details of this time series. Using the maximum value composite approach, the CVI, NDVI, PSRI, and VH time series were merged to form a new comprehensive time series containing 20 time points. This integrated time series lays the foundation for time series classification (TSC).

These raster images [i.e., average monthly precipitation (PRECIP), average monthly temperature (TEMP), SRTM elevation (ELE), soil organic carbon content (Org_Carbon), and total nitrogen content (Total_N)] were classified for choropleth maps using the Jenks breaks classification method. The Jenks breaks method optimizes class arrangement by minimizing within-group variance and maximizing between-group variance, effectively identifying natural data groupings.

The number of Jenks breaks was determined when the Goodness of Variance Fit exceeded 0.9 [22]. In addition to these choropleth maps, the village and town boundaries in Yunzhou helped quantitatively analyze the spatial variation and other factors influencing the growth of daylilies. A detailed description of the features or factors is provided in Table S2.

2.2.5. Training and Validation Sample Data

This study used Google Earth and the QGIS Python plugin to select sampling points. A total of 4248 sampling points were randomly generated and manually labeled through visual interpretation based on expert knowledge and the ESA global land cover product at 10 m resolution. The samples were divided using stratified random sampling into two sets for training and validation, with a ratio of 3:1, ensuring that the sets were mutually exclusive. These samples include eight categories: daylily, other crops, tree cover, shrubland, grassland, wetland, built-up areas, and waterbody.

2.3. Methodology

The proposed methodological framework comprises seven operational phases: (1) data preprocessing involving raster discretization, multisource remote-sensing-index time-series construction, and training-validation sample generation; (2) Principal Component Analysis (PCA) and Simple Non-Iterative Clustering (SNIC) for multitemporal image processing; (3) a classification based on Supervised Time-Series Forest (STSF) for precise delineation of daylily cultivation areas, accompanied by rigorous classification accuracy assessment; (4) quantification of spatial heterogeneity and identification of driving factors analyzing with a geographical detector; (5) management zone partitioning via spatial generalized fuzzy c-means (SGFCM) clustering with spatial autocorrelation constraints; and (6) sys-

tematic validation of zoning rationality through temporal growth-stage profiling and dominant-factor dominance analysis. Figure 2 visually summarizes the comprehensive technical workflow.

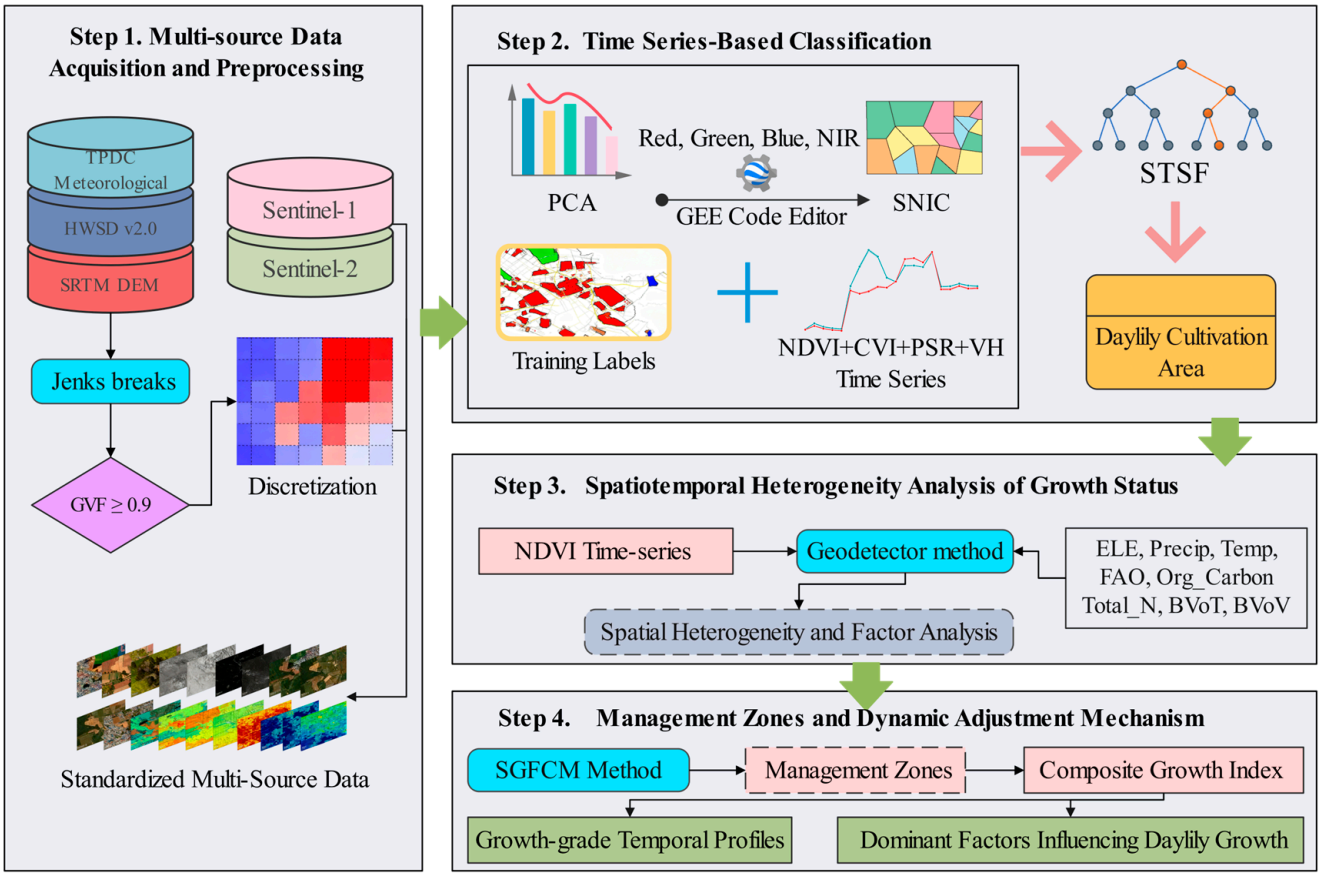


Figure 2. The workflow of this study. Note: GVF, Goodness of Variance Fit; PCA, Principal Component Analysis; NDVI, Normalized Difference Vegetation Index; PSRI, Plant Senescence Reflectance Index; CVI, Chlorophyll Vegetation Index; SNIC, Simple Non-Iterative Clustering; STSF, Supervised Time-Series Forest; TPDC, National Tibetan Plateau Data Center; HWSD v2.0, Harmonized World Soil Database version 2.0.

2.3.1. Reconstructing Temporal Patterns for Classification

To investigate the temporal patterns of land cover, we used a pixel-based stack of various remote-sensing indices derived from Sentinel-1 and Sentinel-2 imagery in conjunction with the training samples. We integrate heterogeneous remote-sensing indices (CVI, NDVI, PSRI, and VH) across five growth stages. Each index's temporal trajectory (five stages) is interleaved to form a 20-dimensional time series, preserving both spectral uniqueness and temporal dynamics for downstream classification (Figure 3).

Water bodies and buildings exhibit distinct morphological signatures within the time-series domain, and a comparative analysis revealed divergent temporal trajectories between NDVI and VH indices among land-cover types. A temporal focal analysis identified the maximum discriminative power of indices during the flowering stage. We subsequently applied these temporal patterns to establish a land-cover classification framework.

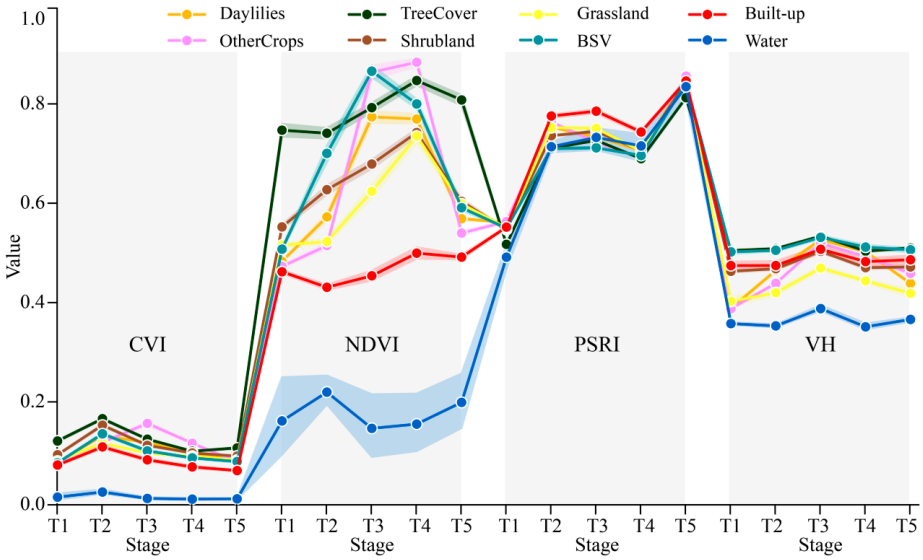


Figure 3. Temporal variations in multiple remote sensing indices across all classes.

2.3.2. Superpixels Segmentation

To improve spatial consistency and reduce noise before classification, the SNIC algorithm was applied to segment the time-series imagery (at 10 m resolution, compressed via Principal Component Analysis) into homogeneous superpixels. SNIC was chosen for its computational efficiency, low memory footprint, and demonstrated effectiveness in enhancing land-cover classification within the Google Earth Engine (GEE) platform [23]. Key hyperparameters of the SNIC algorithm must be defined prior to segmentation: size, which determines the approximate areal extent of each superpixel, and compactness, which balances spatial proximity against spectral homogeneity. Detailed descriptions of these parameters are provided in reference [12].

A sensitivity analysis was conducted to determine the optimal parameter set and evaluate the robustness of the segmentation. Over four representative test areas, we systematically evaluated a grid of parameter combinations: size = [10, 12, 14, 20] pixels and compactness = [0, 1, 5, 7]. Segmentation quality for each combination was quantitatively assessed using two complementary metrics within the test areas: (1) the within-segment variance (measuring intra-segment homogeneity) and (2) the visual correspondence of segment boundaries with discernible landscape features (e.g., field borders and roads).

2.3.3. Supervised Time-Series Forest Classification

To classify the 20-dimensional phenological time series, we employed a Supervised Time-Series Forest (STSF) classifier. STSF extends the random forest framework by embedding discriminative, interval-based feature extraction within each decision tree. During node splitting, the algorithm evaluates random subsequences of the time series, computing summary statistics (e.g., mean and slope) as candidate features [24]. The split that maximizes the reduction in Gini impurity is selected, defined by the information gain:

$$IG(D_p) = I(D_p) - \sum_{j \in \{L,R\}} \frac{|D_j|}{|D_p|} I(D_j)$$

where $I(\cdot)$ denotes the Gini impurity of the parent node D_p or child nodes D_j. An ensemble of such trees is constructed to form the final model.

This algorithm was implemented using the open-source Python library sktime (version 0.30.1).

For comparison, a standard random forest (RF) classifier served as a non-temporal benchmark. The RF classifier is notable for its high accuracy and robustness against overfitting, making it a widely used ensemble learning technique for crop type and land-use land-cover classification [25,26]. We evaluated three modeling approaches to disentangle the contributions of spatial and temporal feature design: a pixel-based RF (RF + Pixel), an object-based RF applied to superpixels (RF + SNIC), and the proposed object-based STSF (STSF + SNIC). To ensure a fair comparison, the hyperparameters for both the RF + Pixel and RF + SNIC models were independently optimized using a consistent grid-search procedure with 5-fold cross-validation. Key parameters tuned included the number of trees (n_estimators: 100, 200, 300, and 500) and the maximum tree depth (max_depth: 20, 30, 50, and 100). All implementations used established Python libraries (sktime and scikit-learn; version 1.5.0) with hyperparameters optimized via grid search.

2.3.4. Classification Accuracy Assessment

The accuracy of the classifications was evaluated using metrics such as overall accuracy (OA), producer's accuracy (PA), user's accuracy (UA) [27], and the kappa coefficient [28]. McNemar's statistical hypothesis test was used to compare machine-learning classifier models [29]. Rejection of the null hypothesis indicates that statistical evidence suggests significant differences in the performance of the models.

When pixels are used for evaluation, the classification outcomes typically focus on individual pixels, overlooking the classification status and spatial relationships of adjacent pixels. As a result, the metrics derived from this approach, which lacks contextual information, may not accurately reflect the model's capability to classify overall ground features and their spatial distribution. After classification, homogeneous units (objects) with distinct attribute features are generated. Overlap rate (OR) is frequently used to quantify the similarity or dissimilarity between distinct objects, thereby providing a supplementary metric for assessing model performance. We selected five test areas (TA1–TA5) and used the overlap rate (only for daylilies) as an indicator to evaluate model performance. OR was calculated using

$$\text{Overlap Ratio} = \frac{S_{\text{GT}} \bigcap S_{\text{model}}}{S_{\text{GT}} + S_{\text{model}} - S_{\text{GT}} \bigcap S_{\text{model}}} \quad (1)$$

where S_{GT} is the area of the ground truth and S_{model} is the area of the model's output, and $S_{\text{GT}} \bigcap S_{\text{model}}$ is the area of their spatial intersection, which was computed using QGIS.

2.3.5. Growth Monitoring and Spatial Heterogeneity

This study employed the Jenks Breaks classification approach to discretize the continuous NDVI data into four distinct growth grades: G1, poor growth; G2, moderately poor growth; G3, moderately good growth; G4, excellent growth. The composite growth index (CGI) was developed to quantify the spatiotemporal heterogeneity of vegetation growth within geographic clusters. This metric is computed using the dot product of the growth grade point vector C and the area percentage vector A:

$$\text{CGI} = \sum_{i=1}^{N} (C_i A_i) \quad (2)$$

The growth grade point C_i is the score corresponding to growth grade i, with values ranging from 0 to N, where N = 4 in this study indicates the best growth state. A_i is the area proportion of growth grade i within a specific cluster, with values ranging from 0 to 1, adhering to the conservation constraint $\sum_{i=1}^{N} A_i = 1$. Extending the CGI to time series provides the growth-grade temporal profile line, which reveals the dynamic changes in daylily growth.

This study employed the GeoDetector method to systematically investigate the mechanisms influencing spatial heterogeneity in daylily growth. The methodology quantifies spatial stratified heterogeneity to reveal how environmental and anthropogenic factors affect growth. We operate under the fundamental spatial coupling hypothesis: when an independent variable significantly influences a dependent variable, its spatial distribution patterns should couple significantly.

In this study, the spatial heterogeneity of growth dynamics, as indicated by the NDVI, was evaluated with respect to eight environmental and agronomic factors: ELE, Precip, Temp, FAO, Org_Carbon, Total_N, BVoT, and BVoV. The relative influence of these factors was quantified using a q-value metric ranging from 0 to 1, where higher q-values indicate that the independent variable has a stronger explanatory power in accounting for the spatial variability of NDVI. Statistically significant factors ($p < 0.05$) were subsequently prioritized as critical determinants for delineating spatially differentiated MZs. To implement the GeoDetector method, we used the QGIS Python plugin (i.e., Geographical Detector, version 1.3.0). The plugin is free to download from https://plugins.qgis.org/plugins/geographical-detector/, accessed on 19 August 2025.

2.3.6. Spatial Constraint Clustering and Management Zones

The SGFCM algorithm was used to produce spatially adaptive clustering and MZs. The SGFCM algorithm incorporates spatial neighborhood constraints into the clustering process, thereby ensuring that the resulting clusters are spatially contiguous and coherent. The SGFCM algorithm requires selecting appropriate parameters, such as the number k of clusters, the fuzziness degree m, and the spatial weighting parameters alpha and beta. Cluster number determination was performed using the elbow criterion, which locates the optimal elbow point by analyzing the rate of change in the variance metrics SSB (between-cluster sum of squares) and SSW (within-cluster sum of squares). The parameter m controls the degree of fuzziness in the clustering results. Increasing m leads to fuzzier clusters, where data have more equal membership across clusters. In the R package geocmeans (version 0.3.4), the default fuzziness degree is m = 1.5, which we adopted. The alpha parameter determines the weight of the spatial dimension (lagged values) used to calculate the membership matrix and the cluster centers. The beta parameter controls the strength of the modification applied to the membership matrix at each iteration, which helps accelerate convergence and produce results that are less fuzzy. The parameters alpha and beta are determined using the grid search method, and the clustering results are validated using the silhouette score.

Implementing the SGFCM algorithm generates several zones with data coherence and spatial coherence. The spatial weight matrix employed in this study was constructed using the Queen contiguity rule combined with the row-standardization method. The clustering results are interpreted through two approaches: constructing a temporal profile by calculating growth grade points and identifying the dominant influencing factor, with both relying on the area proportion.

3. Results

3.1. Segmentation Results

A scree-plot analysis indicated that the first six principal components collectively explained over 96.6% of the total spectral variance; these were therefore selected as the input for the subsequent SNIC algorithm. Guided by the spatial resolution of the base imagery and the characteristic dimensions of field borders in the study area, the SNIC algorithm was parameterized as follows: size = 12, compactness = 5, connectivity = 8, and neighborhood size = 256. These parameters yielded segmentation results that adhered

closely to visible field boundaries (Figure 4). The segmentation process generated a total of 216,054 superpixels across the study area. The objects exhibited considerable heterogeneity in size, with an average of 70 pixels per superpixel. This variation in superpixel dimensions reflects the inherent diversity in the shape, size, and spatial arrangement of ground features—particularly the fragmented nature of agricultural plots within the study region.

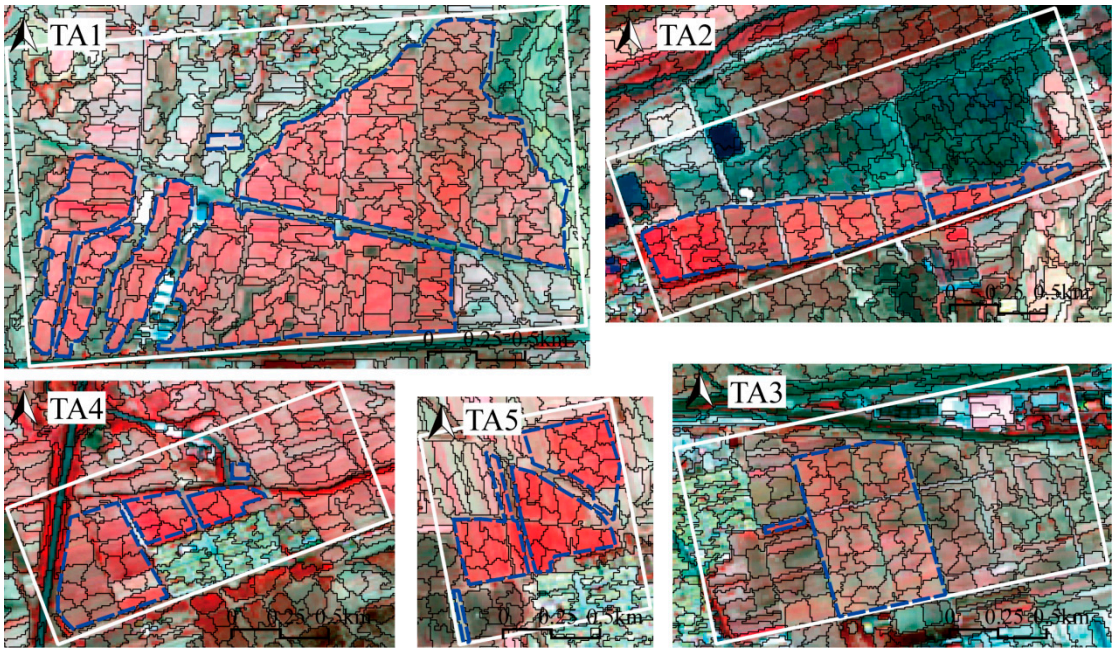


Figure 4. Superpixel segmentation results of time-series images using the SNIC algorithm. The underlying images are false-color composites (NIR, red, and green). The solid white line delineates the boundary of the test area, while the dashed blue line indicates the boundary of the daylily planting region.

3.2. Accuracy Assessment

The three models demonstrated comparable performance in overall accuracy (OA) and Kappa coefficient (Table 2). Among them, the STSF + SNIC model achieved the highest OA (0.941), slightly outperforming the RF + Pixel (0.928) and RF + SNIC (0.931) models. For the target daylilies class, the STSF + SNIC configuration also yielded the highest user's accuracy (UA: 0.966) and producer's accuracy (PA: 0.953) (Figure 5). Notably, its object-based overlap rate (OR) reached 0.886, representing an improvement of 5.4% and 8.0% over the RF + SNIC (0.832) and RF + Pixel (0.806) models, respectively.

Table 2. Performance of the three models.

Model	OA	UA	PA	Kappa	OR
RF + Pixel	0.928	0.952	0.918	0.921	0.806
RF + SNIC	0.931	0.951	0.918	0.923	0.832
STSF + SNIC	0.941	0.958	0.935	0.934	0.886

This gain in spatial alignment extends beyond a statistical increment; it enhances the practical utility of the output for agricultural management. The higher OR reflects superior geometric fidelity in field boundary delineation, which directly translates into more reliable parcel-level area estimation. Accurate area assessment is fundamental for key management decisions, including yield forecasting, precise allocation of inputs (e.g., water, fertilizers), and verification for subsidy or compliance purposes.

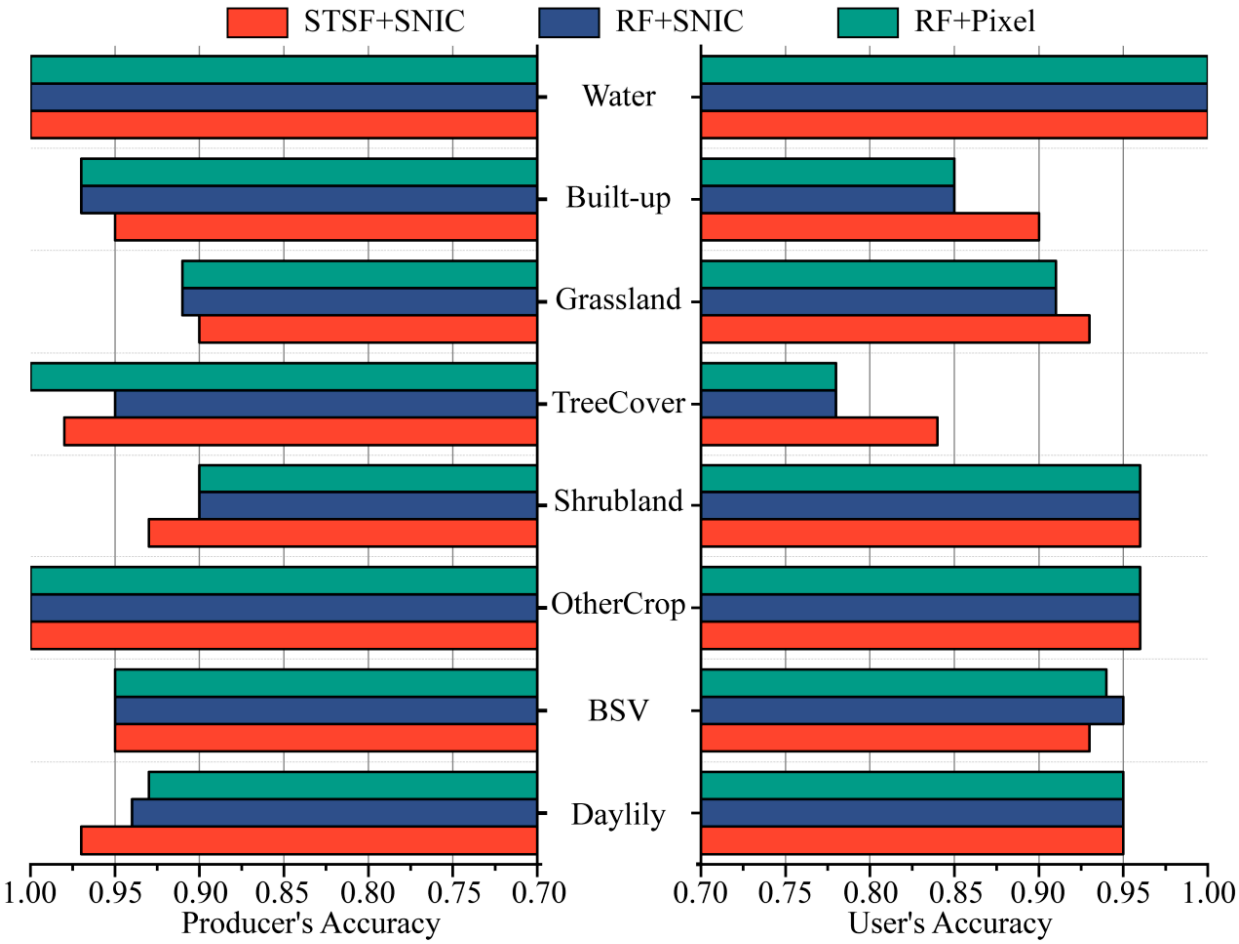


Figure 5. Comparative evaluation of producer accuracy (PA) and user accuracy (UA) across three classification models for eight land cover types.

The differences in classification outcomes produced by the three models were evaluated using McNemar's chi-squared test with continuity correction (Table 3) and a significance level of 0.05. The test confirms that no statistically significant difference exists between the models' performances. The null hypothesis was not rejected. The evaluation metric based on the pixel-based confusion matrix lacks a holistic assessment that incorporates spatial relationships, meaning that, while the confusion matrix provides information on the classification accuracy of individual pixels, it does not fully capture the overall performance of the model in terms of how well the model accounts for the spatial distribution and relationship between pixels in the image. As illustrated in Figure 6, the OR metric more accurately emphasizes the superiority of the STSF + SNIC model, exhibiting enhanced precision in detecting the boundaries of daylily planting areas and effectively mitigating salt-and-pepper noise.

Table 3. Evaluation of differences in classification outcomes of three models via McNemar's chi-squared test.

		UA		PA	
		χ^2	*p*-Value	χ^2	*p*-Value
RF + Pixel	RF + SNIC	0.5224	0.4698	0.5258	0.4683
	STSF + SNIC	0.5105	0.4749	0.5176	0.4718
STSF + SNIC	RF + SNIC	0.5113	0.4745	0.5137	0.4735

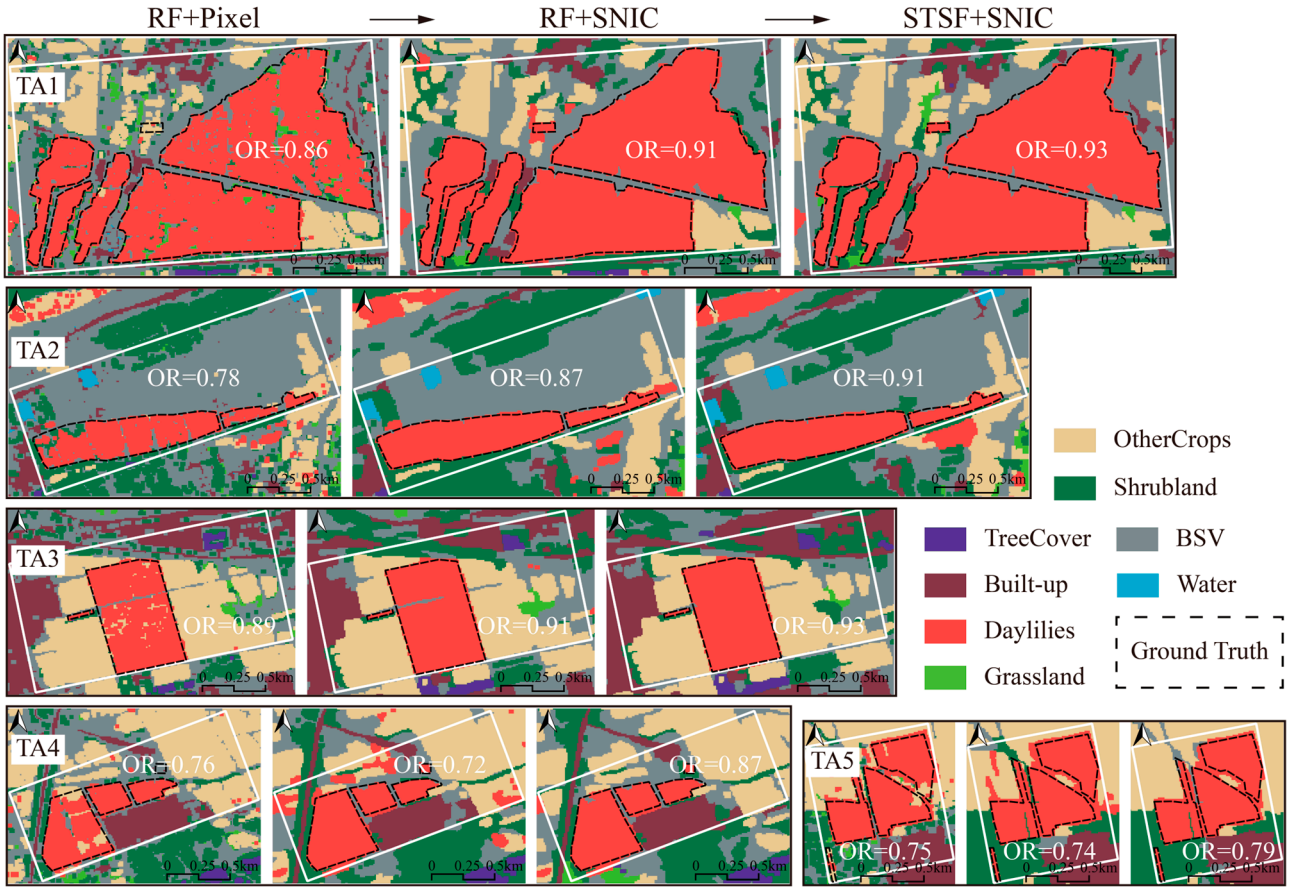


Figure 6. Comparative analysis of three classification models' performance on overlap rate (OR) across five heterogeneous test areas. The solid white line delineates the boundary of each test area, while the dashed black line indicates the boundary of the daylily planting region.

3.3. NDVI Variations and Spatial Heterogeneity in Daylily Growth

We employed the Jenks natural breaks method to classify and map daylily growth grades across five phenological stages (see breakpoints in Figure S1). NDVI values were lowest during the spring-seedling stage (median = 0.48; IQR = 0.47–0.49), corresponding to sparse canopy development. A slight increase occurred at the bolting-budding stage (median = 0.50; IQR = 0.47–0.54), coinciding with stem elongation and bud formation. Heterogeneity in NDVI peaked during the picking stage (median = 0.70; IQR = 0.62–0.80), primarily driven by staggered flowering phenology and selective bud harvesting. Following picking, canopy closure led to the maximum observed NDVI values (median = 0.77; IQR = 0.71–0.82). By the autumn seedling stage, NDVI had declined significantly (median = 0.55; IQR = 0.53–0.58) due to seasonal environmental constraints (Figure S2).

Spatial autocorrelation analysis revealed distinct patterns across these stages (Figure 7D). Weak autocorrelation (Moran's I = 0.359) during initial growth indicated high sensitivity to microenvironmental variation. Spatial homogeneity peaked at the bolting-budding stage (I = 0.749) as canopy development buffered local microvariability. Subsequently, autocorrelation decreased progressively from the picking to the autumn seedling stage (from 0.617 to 0.547), reflecting heightened heterogeneity attributable to autumn climatic variability and diminished management inputs (Figure S3).

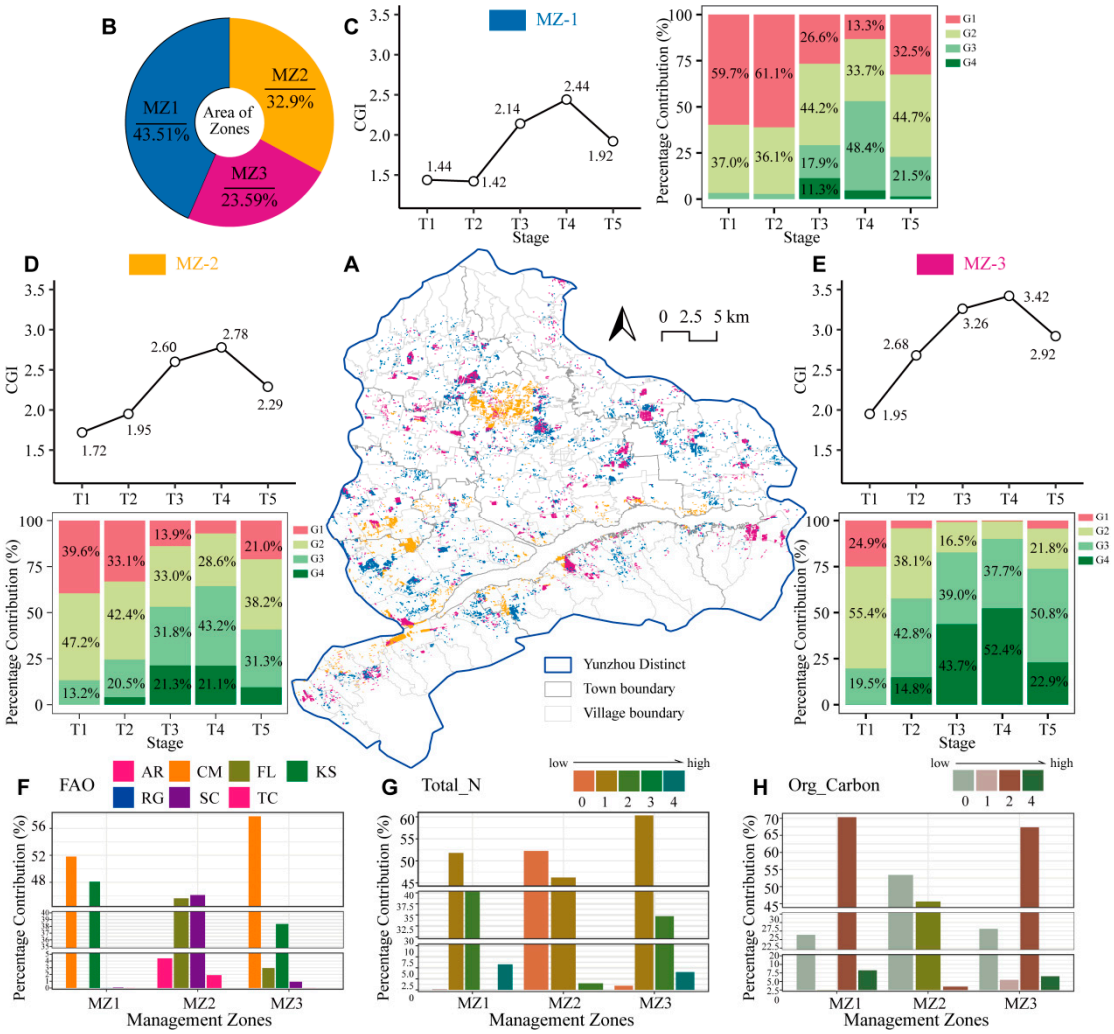


Figure 7. Panel (**A**) presents the spatial distribution map of three management zones (MZ1, MZ2, and MZ3). Panel (**B**) shows a pie chart illustrating the area proportions of these three management zones. Panels (**C**–**E**) depict the temporal profiles of growth grades and stacked area percentage charts for four growth grades across the management zones. Panel (**F**) details the area proportions of various soil types within the three management zones, including arenosols (ARs), cambisol (CM), fluvisol (FL), kastanozem (KS), regosol (RG), solonchak (SC), and technosol (TC). Panel (**G**) outlines the area proportions of graded total carbon content in the three management zones, categorized as extremely low (EL), low (L), moderate (M), high (H), and extremely high (EH). Panel (**H**) provides the area proportions of graded organic carbon content within the three management zones.

3.4. Impacts of Environmental and Anthropogenic Factors

Prior to GeoDetector analysis, all numerical variables were discretized using the Jenks natural breaks method into four to five classes for visualization as choropleth maps (Figure S4). This preprocessing step was necessary to generate the discrete input data required by the GeoDetector model. The categorical variable (FAO) was excluded from this discretization procedure.

GeoDetector analysis revealed that the dominant factors influencing NDVI exhibited strong stage-specific dependence throughout the daylily growing season (Figure S5). At the spring-seedling stage, growth was primarily driven by township-level management practices (BVoT, q = 3.4%, $p < 0.001$) and soil organic carbon (q = 1.9%, $p < 0.05$), whereas climatic factors were insignificant, highlighting the sensitivity of early growth to local management and soil fertility. During the bolting-budding and picking stages, all eight environmental and anthropogenic factors became significant ($p < 0.05$), indicating that

growth in these phases was co-regulated by temperature, water, nutrients, and multi-level governance (BVoT, BVoV). Notably, village-level management (BVoV) showed the highest explanatory power during this period (q = 17.3–22.8%).

A shift in driving factors occurred post-picking. In the post-picking stage, the influence of climatic and topographic factors became non-significant, with growth subsequently governed by soil parameters (organic carbon and total nitrogen) and multi-level management, which regulated nutrient retention and stem senescence patterns. By the autumn-seedling stage, the effect of village-level management (BVoV) diminished, and growth relied mainly on sustained soil nutrient supply (organic carbon and total nitrogen) and farm-scale management practices (FAO, q = 3.8%).

Overall, township-level management (BVoT) maintained significant influence across all stages ($p < 0.001$), underscoring its overarching regulatory role. The growth dynamics of daylilies were primarily governed by the synergistic effects of multiple factors under intensive anthropogenic intervention, providing a theoretical basis for implementing precision zone management.

3.5. Hyperparameter Tuning and Clustering Results

The optimal number of clusters for the SGFCM model was determined as three based on the elbow criterion. Both the BSS and WSS indicated a statistically optimal elbow point at K = 3, beyond which the marginal improvement diminished (Figure S6). We employed a grid-search approach to optimize the spatial and fuzzy parameters of the model, scanning the greedy search space $\alpha \in [0.1, 0.9]$ and $\beta \in [0.1, 0.9]$ with a step size of 0.05. The optimal parameter combination was identified as $\alpha = 0.2$ and $\beta = 0.75$, which maximized the silhouette coefficient at a value of 0.471, indicating a reasonable and robust cluster structure for subsequent management zone analysis.

The three primary zones of growth patterns reflect the impact of variations in the daylily distribution and temporal changes resulting from three key factors: FAO, Org_Carbon, and Total_N, which continuously exert a significant influence on the NDVI. The three zones account for 43.51%, 32.9%, and 23.59% of the total area, respectively, indicating that no regions have extremely large or extremely small areas (Figure 7A,B).

3.6. Management Zones and Their Rationality

The temporal growth-grade profiles of three MZs (MZ1-3), derived from CGI analysis, revealed distinct spatiotemporal dynamics in daylily development across five growth stages (T1–T5) (Figure 7C–E). We quantified the proportional distributions of soil types, total nitrogen content grades, and organic carbon content grades within these MZs (Figure 7F–H). Subsequent analysis integrated temporal growth patterns with edaphic factors to characterize zone-specific cultivation patterns.

The spatiotemporal growth patterns differed significantly between MZs. MZ1 had bimodal dynamics, reaching peak values at T3 (CGI = 2.14) and T4 (CGI = 2.44), with a subsequent 21.3% decline in T5 (CGI = 1.92). This growth instability was associated with distinct edaphic drivers: cambisol (51.8% coverage) and kastanozem (48.1% coverage) soils competed hydrologically through differential water retention capacity and calcium carbonate deposition processes. Furthermore, the widespread distribution of moderate organic carbon (70.3% coverage) coupled with low nitrogen availability (51.8% coverage) contributed to nutrient flux imbalances, highlighting the need for stage-specific fertilization strategies.

MZ2 exhibited linear growth through T4 (CGI = 2.78), retaining 82.4% of its maximum CGI at T5. The fluvisol–solonchak soil complex (45.6% versus 46.1% coverage) had a dual functionality: fluvisols offer mineral-rich substrates, whereas solonchaks necessitate

targeted salinity mitigation. Extremely low nutrient status predominated, with 52.3% and 53.4% of areas having deficient nitrogen and organic carbon, respectively, indicating poor nutrient availability that could impair sustainable growth. These findings suggest that productivity could be enhanced by precision nitrogen supplementation integrated with soil-moisture-based irrigation protocols.

MZ3 underwent superior growth, reaching a peak CGI of 3.42 at T4 due to synergistic soil composition. The dominant cambisols (57.8%) and kastanozems (38.3%) formed stable aggregates that coupled with moderate organic carbon (67.4% coverage) and balanced nitrogen distribution (low, 60.3%; moderate, 34.7%; and exceptionally high, 4.0%) to sustain an efficient C-N cycling system supporting metabolic requirements during critical growth phases. However, the 38.3% kastanozem content necessitates monitoring calcic horizon dynamics to mitigate alkaline accumulation in the rhizosphere.

We quantified growth heterogeneity using Kruskal–Wallis H tests comparing NDVI distributions between MZs (MZ1–MZ3) throughout phenological stages (T1–T5). Spatially independent NDVI observations (MZ1, n = 13213; MZ2, n = 6691; and MZ3, n = 8470), where n denotes the parcel count, were verified through Moran's I analysis. Statistical analysis revealed significant interzone heterogeneity ($p < 0.0001$) between the MZs across all five growth stages (Figure 8A). The global Moran's I statistic (queen contiguity weighting) quantified spatial autocorrelation patterns across phenological stages, revealing a strong positive spatial autocorrelation (global Moran's I = 0.603 ± 0.12, range 0.328–0.797, $p < 0.001$) with temporal consistency (Figure 8B). These findings indicate that, within designated MZs, the key attributes of daylily parcels undergo significant spatial clustering (growth vigor and soil characteristics), manifesting spatial autocorrelation of homogeneous attributes.

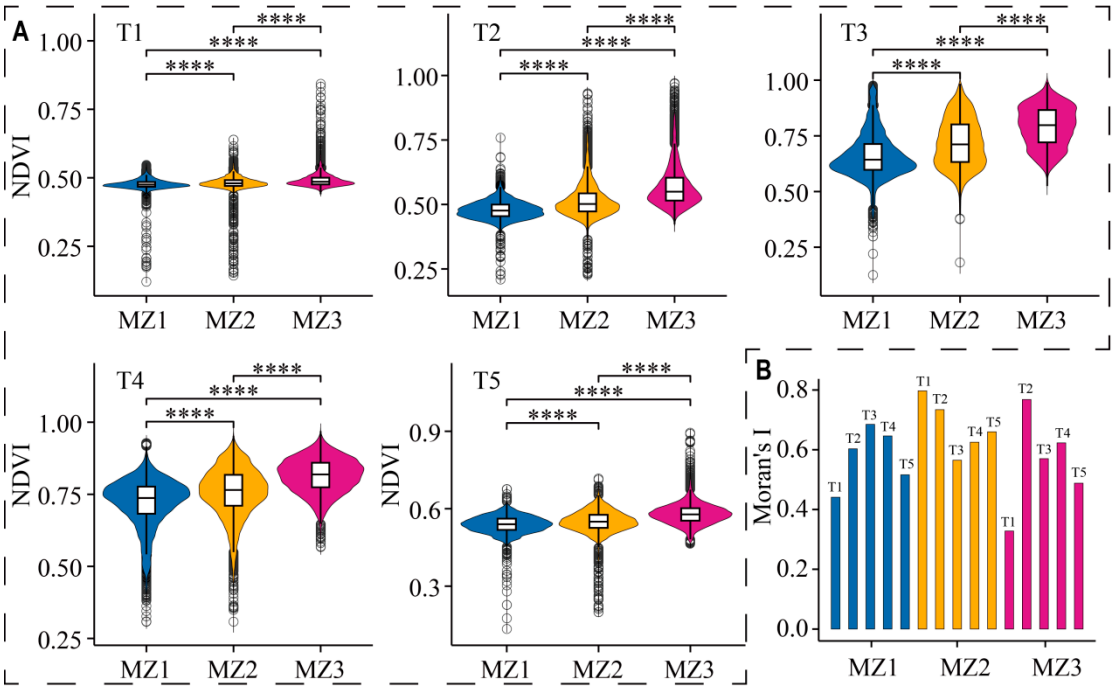


Figure 8. Analysis of differences among three management zones. Panel (**A**) employs the Kruskal–Wallis H test to compare NDVI values across the three management zones (MZs) at five growth stages, with significance levels indicated as $p \leq 0.0001$ (****). Panel (**B**) presents the Global Moran's I index for the three management zones across the five growth stages, assessing spatial autocorrelation and clustering patterns of growth grades within each zone.

4. Discussion

TSC classifiers are specifically designed to handle time-series data and can effectively capture the temporal dynamics and changes in remote-sensing data over time. These classifiers leverage temporal contextual information to resolve classification ambiguities arising from land-cover types that exhibit comparable spectral signatures at individual time points but divergent temporal profiles. Recent studies have validated that this approach enhances the accuracy and reliability of classification results in such contexts [29,30]. The STSF classifier extracts features using time windows. Compared with nontemporal classifiers (e.g., conventional random forest), it enables the temporal dependencies between sequential observations to be systematically exploited, thereby reducing the adverse effects of local noise and outliers on classification boundaries [24]. This robustness is critical in remote sensing, where data may be affected by various factors, such as atmospheric conditions, sensor malfunctions, or environmental changes.

TSC classifiers such as STSF are computationally intensive, particularly when processing large-scale remote-sensing data. All models (RF + Pixel, RF + SNIC, and STSF + SNIC) were implemented on identical hardware (six-core 2.8 GHz processor, 16 GB RAM). Even with SNIC-based superpixel segmentation—which reduces data volume and computational load—the STSF + SNIC model required approximately ~33,195 s for completion, compared with only 742 s for RF + Pixel and 542 s for RF + SNIC. This substantial computational burden may therefore constrain the use of STSF in real- or near-real-time remote-sensing applications, where rapid processing and decision-making are essential. Nevertheless, in contexts such as perennial crop management (e.g., daylily), where zoning frameworks are designed for long-term, multi-seasonal deployment, the initial investment in a robust and temporally explicit model can be justified. Its enduring operational value not only offsets but may ultimately surpass the associated one-time computational overhead, yielding a net strategic benefit.

The SGFCM algorithm was chosen to delineate MZs owing to its theoretical coherence with the spatial continuity of agricultural landscapes and its empirical effectiveness. Unlike non-spatial classifiers (e.g., k-means), topology-preserving methods (e.g., self-organizing maps), or density-based techniques (e.g., DBSCAN), SGFCM explicitly integrates neighborhood constraints, ensuring that resulting zones are spatially contiguous—a prerequisite for deriving operational management units. Moreover, its fuzzy-membership framework naturally accommodates gradual transitions in agro-environmental variables, better representing continuous landscape gradients than crisp classification schemes. By incorporating spatial constraints, the SGFCM model extends conventional fuzzy clustering, increasing the likelihood that adjacent locations belong to the same zone. This approach effectively captures spatially correlated drivers such as growth vigor and soil properties, thereby mitigating artifacts arising from spatial autocorrelation. The MZs delineated in this study exhibited strong intra-zone homogeneity, reflected by a global Moran's I of 0.600 (Z-score = 106.85, $p < 0.001$). For comparison, a conventional fuzzy c-means baseline yielded a substantially lower Moran's I of 0.433 (Z-score = 77.07, $p < 0.001$). This result indicates that SGFCM enhances spatial coherence among daylily patches within zones, reducing spatial fragmentation by 27.8%—consistent with earlier findings on the ability of spatially constrained clustering to suppress within-zone heterogeneity [31–33].

The advancement of remote-sensing technology has significantly enhanced the efficiency of NDVI data. This progress has enabled the monitoring of low-cost, wide-area farmland and provided a robust foundation based on data for demarcating crop-growth MZs [9]. However, using only the NDVI time-series during the critical growth stages of daylilies within a single year may be subject to the impacts of annual climate conditions and pests and diseases, causing significant data fluctuations and thus affecting the stability

of MZ demarcation [34]. In this study, we integrated the NDVI time-series data during the critical growth stages within a year with other multiyear relevant data, such as meteorological and soil characteristic data. This integration effectively enhanced the spatiotemporal representativeness and noise resistance of the fundamental data. Subsequent studies can use the multiyear average NDVI time series data and combine it with field survey data, such as yield and biomass, to validate the results of growth MZ demarcation, ensuring the accuracy and reliability of the zones.

Natural environmental factors (e.g., Org_Carbon, Total_N, ELE, Precip, and Temp) exhibit spatially continuous gradient characteristics and remain relatively stable over extended temporal scales, with their distribution patterns being accurately characterized through remote sensing or field sampling. Crop growth MZs delineated based on these natural factors demonstrate sustained effectiveness and applicability. In contrast, administrative boundaries (e.g., BVoT and BVoV) frequently display abrupt segmentation patterns, exemplified by NDVI leap variations between adjacent villages resulting from management disparities. This study establishes that soil-characteristic indicators (e.g., Org_Carbon, Total_N, and FAO) provide a poorer explanation of NDVI variations than administrative boundary indicators, a limitation primarily attributable to the spatial resolution constraints of raster datasets. Employing higher-resolution soil sensing data or coupling with proximal soil spectroscopy in future studies could refine the explicit integration of soil information. These limitations do not undermine the core findings but underscore the importance of higher-fidelity input data and multi-temporal validation for operational applications.

The GeoDetector analysis effectively identified stage-specific drivers of daylily growth, though the method assumes explanatory variables to be largely independent. In this study, correlations between soil properties and socio-administrative factors may introduce multicollinearity, potentially inflating the individual q-statistics and obscuring causal inference. Nonetheless, the persistently high statistical significance and distinct phenological progression of the detected factors affirm their ecological and agronomic relevance. Future studies could integrate collinearity diagnostics or hybrid modeling frameworks to better disentangle covariate influences. Despite this limitation, the observed spatial heterogeneity provides a robust empirical foundation for delineating management zones.

5. Conclusions

This study developed and validated an integrated analytical framework that synergistically combined time-series classification, object-based image analysis, and spatially constrained clustering to address the persistent challenges of accurate monitoring and precision management. The framework demonstrated superior efficacy in crop identification under complex phenological conditions. The integration of the STSF classifier with SNIC segmentation achieved the highest classification accuracy (overall accuracy = 0.941) and, more importantly, significantly improved the geometric fidelity of delineated planting parcels (overlap rate = 0.886). This advancement directly enhances the practicality of remote-sensing outputs for parcel-level area estimation, which is fundamental for yield forecasting, input allocation, and policy compliance.

This study establishes a direct linkage between high-resolution crop mapping and operational agricultural decision-making. Through the integration of Geographical Detector analysis and SGFCM, we delineated three agronomically coherent MZs that exhibit clear spatial continuity. Compared to conventional non-spatial clustering methods, this approach reduced within-zone fragmentation by 27.8%, thereby yielding practical management units that align more closely with actual field conditions and operational logistics. These zones exhibited significant intra-zone homogeneity and inter-zone heterogeneity in growth vigor (NDVI) across key phenological stages, validated by robust statistical tests

(Kruskal–Wallis H test, $p < 0.0001$; global Moran's I = 0.603 ± 0.12). The analysis revealed that daylily growth dynamics are governed by stage-specific synergies between anthropogenic factors (especially multi-level governance) and intrinsic soil properties (organic carbon, total nitrogen), providing a data-driven theoretical basis for zone-specific management strategies.

Overall, this research establishes a comprehensive remote sensing framework that spans data preprocessing, temporal modeling, classifier evaluation, spatial heterogeneity diagnosis, and management zone optimization. It provides a transferable methodology for supporting sustainable daylily production, reducing land-use inefficiency, and bridging the gap between remote sensing technology and practical agricultural management. The approach presented here holds promise for supporting food security and environmentally informed decision-making in regional agricultural systems.

Supplementary Materials: The following supporting information can be downloaded at: https://www.mdpi.com/article/10.3390/agriculture16050540/s1, Figure S1: The spatial distribution of daylily growth stage classifications across five stages; Figure S2: Analysis of spatiotemporal patterns and spatial autocorrelation in daylily growth; Figure S3: Changes in Moran's I and its significance level; Figure S4: Characterization of key environmental factors across the study area; Figure S5: GeoDetector q statistics; Figure S6: Determination of optimal clustering parameters; Table S1: A comprehensive list of vegetation indices derived from Sentinel-2; Table S2: Key features and influential factors for time-series classification and spatial analysis.

Author Contributions: L.H.: Conceptualization, Methodology, Software, Data curation, Investigation, Writing—original draft, Writing—review and editing, Funding acquisition. J.D.: Conceptualization, Validation, Resources. G.J.: Investigation, Data curation, Visualization. X.L.: Investigation, Data curation. N.Z.: Investigation, Visualization. B.L.: Conceptualization, Validation, Resources. All authors have read and agreed to the published version of the manuscript.

Funding: This work was supported by the Datong Municipal Bureau of Science and Technology [Applied Basic Research Program of Datong City, Grant No. 2025082]; the Department of Education of Shanxi Province [Scientific and Technological Innovation Programs of Higher Education Institutions in Shanxi, Grant No. 2020L0489]; and Shanxi Datong University [Doctoral Research Initiation Project, Grant No. 2019-B-02].

Institutional Review Board Statement: Not applicable.

Data Availability Statement: Data are contained within the article.

Conflicts of Interest: Author Jianwen Duan is affiliated with Shanxi Wanding Space Digital Co., Ltd. Author Baoxing Liang is affiliated with Shanxi Provincial Coal Geology 115 Exploration Institute Co., Ltd. The remaining authors (Liang Han, Gaoyi Ji, Xudong Li, and Nan Zhang) declare that they have no known competing financial interests or personal relationships that could have appeared to influence the work reported in this paper. The involvement of the authors with commercial affiliations was solely in their capacity as researchers.

Abbreviations

The following abbreviations are used in this manuscript:

NDVI	Normalized Difference Vegetation Index
PSRI	Plant Senescence Reflectance Index
CVI	Chlorophyll Vegetation Index
S1	Sentinel-1 SAR
S2	Sentinel-2 MSI
T1	Spring-Seedling Stage
T2	Bolting-Budding Stage

T3	Picking Stage
T4	Post-Picking Stage
T5	Autumn-Seedling Stage
recip	Average Monthly Precipitation
Temp	Average Monthly Temperature
ELE	Elevation
BVoT	Boundary Vectors of Town
BVoV	Boundary Vectors of Village
GVF	Goodness of Variance Fit
PCA	Principal Component Analysis
SNIC	Simple Non-Iterative Clustering
STSF	Supervised Time-Series Forest
TPDC	National Tibetan Plateau Data Center
HWSD v2.0	Harmonized World Soil Database version 2.0
ARs	Arenosols
CM	Cambisol
FL	Fluvisol
KS	Kastanozem
RG	Regosol
SC	Solonchak
TC	Technosol

References

1. Gao, J. White paper on the development of the daylily industry 2023. *China Food Newspaper*, 2023. Available online: https://www.foodscn.cn/jujiao/10129 (accessed on 1 January 2026).
2. Li, W.; Zhang, K.; Liu, J.; Wu, J.; Zhang, Y.; Henke, M. Optimizing daylily (*Hemerocallis citrina* Baroni) cultivation: Integrating physiological modeling and planting patterns for enhanced yield and resource efficiency. *Front. Plant Sci.* **2024**, *15*, 1442485. [CrossRef]
3. Feng, H.; Tao, H.; Li, Z.; Yang, G.; Zhao, C. Comparison of UAV RGB Imagery and Hyperspectral Remote-Sensing Data for Monitoring Winter Wheat Growth. *Remote Sens.* **2022**, *14*, 3811. [CrossRef]
4. Wang, J.; Wang, Y.; Qi, Z. Remote Sensing Data Assimilation in Crop Growth Modeling from an Agricultural Perspective: New Insights on Challenges and Prospects. *Agronomy* **2024**, *14*, 1920. [CrossRef]
5. Chen, S.; Du, T.; Wang, S.; Parsons, D.; Wu, D.; Guo, X.; Li, D. Quantifying the effects of spatial-temporal variability of soil properties on crop growth in management zones within an irrigated maize field in Northwest China. *Agric. Water Manag.* **2021**, *244*, 106535. [CrossRef]
6. de Oliveira Maia, F.C.; Bufon, V.B.; Leão, T.P. Vegetation indices as a Tool for Mapping Sugarcane Management Zones. *Precis. Agric.* **2022**, *24*, 213–234. [CrossRef]
7. Silva, G.R.; Escarpinati, M.C.; Abdala, D.D.; Souza, I.R. Definition of Management Zones Through Image Processing for Precision Agriculture. In Proceedings of the 2017 Workshop of Computer Vision (WVC), Natal, Brazil, 30 October–1 November 2017; pp. 150–154.
8. Rasmussen, J.; Azim, S.; Boldsen, S.K.; Nitschke, T.; Jensen, S.M.; Nielsen, J.; Christensen, S. The challenge of reproducing remote sensing data from satellites and unmanned aerial vehicles (UAVs) in the context of management zones and precision agriculture. *Precis. Agric.* **2021**, *22*, 834–851. [CrossRef]
9. Damian, J.; Pias, H.; Cherubin, M.; Fonseca, A.; Fornari, E.; Santi, A. Applying the NDVI from satellite images in delimiting management zones for annual. *Sci. Agric.* **2019**, *77*, 2020. [CrossRef]
10. Ali, A.; Rondelli, V.; Martelli, R.; Falsone, G.; Lupia, F.; Barbanti, L. Management Zones Delineation through Clustering Techniques Based on Soils Traits, NDVI Data, and Multiple Year Crop Yields. *Agriculture* **2022**, *12*, 231. [CrossRef]
11. Silva, C.d.O.F.; Grego, C.R.; Manzione, R.L.; Oliveira, S.R.d.M.; Rodrigues, G.C.; Rodrigues, C.A.G. Delineation of management zones dealing with low sampling and outliers. *Precis. Agric.* **2025**, *26*, 19. [CrossRef]
12. Shafizadeh-Moghadam, H.; Khazaei, M.; Alavipanah, S.K.; Weng, Q. Google Earth Engine for large-scale land use and land cover mapping: An object-based classification approach using spectral, textural and topographical factors. *GISci. Remote Sens.* **2021**, *58*, 914–928. [CrossRef]
13. Mercier, A.; Betbeder, J.; Baudry, J.; Le Roux, V.; Spicher, F.; Lacoux, J.; Roger, D.; Hubert-Moy, L. Evaluation of Sentinel-1 & 2 time series for predicting wheat and rapeseed phenological stages. *ISPRS J. Photogramm. Remote Sens.* **2020**, *163*, 231–256. [CrossRef]

14. Yang, L.; Wang, L.; Abubakar, G.A.; Huang, J. High-Resolution Rice Mapping Based on SNIC Segmentation and Multi-Source Remote Sensing Images. *Remote Sens.* **2021**, *13*, 1148. [CrossRef]
15. Sadeghi-Tehran, P.; Virlet, N.; Ampe, E.M.; Reyns, P.; Hawkesford, M.J. DeepCount: In-Field Automatic Quantification of Wheat Spikes Using Simple Linear Iterative Clustering and Deep Convolutional Neural Networks. *Front. Plant Sci.* **2019**, *10*, 1176. [CrossRef]
16. Huang, X.; Wang, H.; Li, X. A multi-scale semantic feature fusion method for remote sensing crop classification. *Comput. Electron. Agric.* **2024**, *224*, 109185. [CrossRef]
17. Chen, D.; Hu, H.; Liao, C.; Ye, J.; Bao, W.; Mo, J.; Wu, Y.; Dong, T.; Fan, H.; Pei, J. Crop NDVI time series construction by fusing Sentinel-1, Sentinel-2, and environmental data with an ensemble-based framework. *Comput. Electron. Agric.* **2023**, *215*, 108388. [CrossRef]
18. Bauer-Marschallinger, B.; Cao, S.; Navacchi, C.; Freeman, V.; Reuß, F.; Geudtner, D.; Rommen, B.; Vega, F.C.; Snoeij, P.; Attema, E.; et al. The normalised Sentinel-1 Global Backscatter Model, mapping Earth's land surface with C-band microwaves. *Sci. Data* **2021**, *8*, 277. [CrossRef] [PubMed]
19. Nasiri, V.; Le Bris, A.; Darvishsefat, A.A.; Moradi, F. Integration of radar and optical sentinel images for land use mapping in a complex landscape (case study: Arasbaran Protected Area). *Arabian J. Geosci.* **2022**, *15*, 1759. [CrossRef]
20. Peng, S. *1-km Monthly Mean Temperature Dataset for China (1901–2024)*; National Tibetan Plateau/Third Pole Environment Data Center: Beijing, China, 2025. [CrossRef]
21. Peng, S. *1-km Monthly Precipitation Dataset for China (1901–2024)*; National Tibetan Plateau/Third Pole Environment Data Center: Beijing, China, 2025. [CrossRef]
22. Vohnoutová, M.; Sedláková, A.; Symonová, R. Abandoning the Isochore Theory Can Help Explain Genome Compositional Organization in Fish. *Int. J. Mol. Sci.* **2023**, *24*, 13167. [CrossRef]
23. Tassi, A.; Vizzari, M. Object-Oriented LULC Classification in Google Earth Engine Combining SNIC, GLCM, and Machine Learning Algorithms. *Remote Sens.* **2020**, *12*, 3776. [CrossRef]
24. Cabello, N.; Naghizade, E.; Qi, J.; Kulik, L. Fast and Accurate Time Series Classification Through Supervised Interval Search. In Proceedings of the 2020 IEEE International Conference on Data Mining (ICDM), Sorrento, Italy, 17–20 November 2020; pp. 948–953.
25. Vizzari, M.; Lesti, G.; Acharki, S. Crop classification in Google Earth Engine: Leveraging Sentinel-1, Sentinel-2, European CAP data, and object-based machine-learning approaches. *Geo-Spat. Inf. Sci.* **2024**, *28*, 815–830. [CrossRef]
26. Li, M.; Ma, L.; Blaschke, T.; Cheng, L.; Tiede, D. A systematic comparison of different object-based classification techniques using high spatial resolution imagery in agricultural environments. *Int. J. Appl. Earth Obs. Geoinf.* **2016**, *49*, 87–98. [CrossRef]
27. Congalton, R.G. A review of assessing the accuracy of classifications of remotely sensed data. *Remote Sens. Environ.* **1991**, *37*, 35–46. [CrossRef]
28. Cohen, J. A coefficient of agreement for nominal scales. *Educ. Psychol. Meas.* **1960**, *20*, 37–46. [CrossRef]
29. Belgiu, M.; Csillik, O. Sentinel-2 cropland mapping using pixel-based and object-based time-weighted dynamic time warping analysis. *Remote Sens. Environ.* **2018**, *204*, 509–523. [CrossRef]
30. Yan, J.; Wang, L.; Song, W.; Chen, Y.; Chen, X.; Deng, Z. A time-series classification approach based on change detection for rapid land cover mapping. *ISPRS J. Photogramm. Remote Sens.* **2019**, *158*, 249–262. [CrossRef]
31. Kupfer, J.A.; Gao, P.; Guo, D. Regionalization of forest pattern metrics for the continental United States using contiguity constrained clustering and partitioning. *Ecol. Inf.* **2012**, *9*, 11–18. [CrossRef]
32. Ouazaa, S.; Jaramillo-Barrios, C.I.; Chaali, N.; Amaya, Y.M.Q.; Carvajal, J.E.C.; Ramos, O.M. Towards site specific management zones delineation in rotational cropping system: Application of multivariate spatial clustering model based on soil properties. *Geoderma Reg.* **2022**, *30*, e00564. [CrossRef]
33. Chen, Y.; Liu, Q.; Yang, J.; Cheng, X.; Deng, M. Spatially constrained statistical approach for determining the optimal number of regions in regionalization. *Int. J. Geogr. Inf. Sci.* **2024**, *38*, 2108–2147. [CrossRef]
34. Kasimati, A.; Psiroukis, V.; Darra, N.; Kalogrias, A.; Kalivas, D.; Taylor, J.A.; Fountas, S. Investigation of the similarities between NDVI maps from different proximal and remote sensing platforms in explaining vineyard variability. *Precis. Agric.* **2023**, *24*, 1220–1240. [CrossRef]

Disclaimer/Publisher's Note: The statements, opinions and data contained in all publications are solely those of the individual author(s) and contributor(s) and not of MDPI and/or the editor(s). MDPI and/or the editor(s) disclaim responsibility for any injury to people or property resulting from any ideas, methods, instructions or products referred to in the content.